Short-crested wave interaction with a concentric porous cylindrical structure

Hao Song and Longbin Tao *

Griffith School of Engineering, Gold Coast campus, Griffith University, QLD4222, Australia

Abstract

In this paper, theoretical study is carried out to investigate the general 3D short-crested wave interaction with a concentric two-cylinder system. The interior cylinder is impermeable and the exterior cylinder is thin in thickness and porous to protect the interior cylinder. Both cylinders are surface-piercing and bottom mounted. Analytical solution is derived based on the linear potential theory. The effects of the wide range wave parameters and structure configuration including porosity of the exterior cylinder and the annular spacing on the wave forces, surface elevations and the diffracted wave contours are examined.

Key words: short-crested wave, wave diffraction, vertical cylinder

1 Introduction

Porous layers are often constructed to protect coastal and offshore structures from the direct wave impact. Such porous structures, for instance, rock-filled porous

* Corresponding author. Tel.: +61 755529093; fax: +61 755528065.
Email address: l.tao@griffith.edu.au (Longbin Tao).

breakwaters outside harbours, concentric porous outer protective structure with the main structure in its interior, are very effective in reducing both the transmitted and reflected wave heights, as well as hydrodynamic forces acting on the protected structures. One example of these applications in offshore engineering is the successful Ekofisk gravity offshore structure in the North Sea (see Fig. 1). For these reasons, wave motion through a porous structure has attracted considerable attention among researchers in coastal and ocean engineering (e.g., [1]).

[Fig. 1 about here.]

Taylor [2] showed that for the fluid flow passing through the porous boundary, it is normally assumed that the pressure difference between the two sides of the porous boundary is proportional to either (a) the square of the flow velocity perpendicular to the boundary, or (b) the flow velocity perpendicular to the boundary depending on the configuration or material of the porous wall and relevant parameters. It is commonly accepted in the study of flow in porous media that wire gauze and perforated sheets have approximately the property of (a) (e.g., [3, 4]), while materials with very fine pores have properties more like (b) (e.g., [5–7]).

In addition to the porous wavemaker theory of Chwang [5] and subsequent works, investigations on waves past a porous structure are primarily been concentrated on the hydrodynamic effects of a porous structure on the incoming wave trains, or wave impact on porous structures as a breakwater in a harbour (e.g., [6–8]). In most cases, Darcy's law for a homogeneous porous medium has been applied. Yu and Chwang [6] investigated the resonance in a harbour with porous breakwaters with the wave entering at an arbitrary angle. Yu and Chwang [7] performed extensive study on the transmission characteristics of waves past a porous structure. The wave behaviour within the porous medium was also investigated. It was found

that there is an optimum thickness for a porous structure beyond which any further increase of the thickness may not lead to an appreciable improvement in reducing its transmission and reflection characteristics. Wang and Ren [9] also studied the performance of a flexible and porous breakwater. Additional related work can be found in the review article of Chwang and Chan [8].

Though considerable research efforts have been devoted to the wave interaction with porous structures, relatively limited attention has been focused on the wave diffraction by a concentric bottom-mounted porous cylindrical structure, where the interior cylinder is impermeable and the exterior cylinder is thin and porous. Wang and Ren [10] investigated analytically the plane wave diffraction by the above-mentioned system. They found that hydrodynamic forces on the interior cylinder as well as wave amplitudes around the windward side of the interior cylinder are reduced when compared to the case of a direct wave impact on the interior cylinder. As the annular spacing increases, the hydrodynamic force on the interior cylinder decreases. It was further shown that, as the porosity of the exterior cylinder increases, the hydrodynamic force on the interior cylinder increases. Li et al. [11] reported similar results from their experimental and numerical study with only partial porosity in the circumferential direction of the exterior cylinder. Darwiche et al. [12] also studied the wave diffraction by a two-cylinder system, with the exterior cylinder being porous only in the vicinity of free surface. Williams and Li [13] further extended the work by mounting the interior cylinder on a storage tank.

The aforementioned studies on ocean surface wave interaction with a vertical porous cylindrical structure are generally two-dimensional. In reality, however, the ocean waves are more complex, and better described by three-dimensional short-crested waves. They also commonly arise, for example, from the oblique interaction of two travelling plane waves or intersecting swell waves, from the reflection of waves at

non-normal incident off a vertical seawall, as well as from diffraction about the surface boundaries of a structure of finite length. Such waves are of paramount importance in coastal and offshore engineering design. Unlike the plane waves propagating in a single direction, and the standing waves fluctuating vertically in a confined region, short-crested waves can be doubly periodic in two horizontal directions, one in the direction of propagation and the other normal to it [14].

Theoretical analysis on short-crested wave interaction with a vertical cylinder can be found in [15–17]. Zhu [15] presented an analytic solution to the diffraction problem for a circular cylinder in short-crested waves using linear potential wave theory and found that the pressure distribution and wave run-up on the cylinder were quite different from those of plane incident waves. Their patterns become very complex as ka (i.e., total incident wave number k times cylinder radius a) becomes large. The hydrodynamic forces on the cylinder become smaller as the short-crestedness of the incident waves increases. Subsequently, Zhu and Moule [16] observed that the hydrodynamic force induced by short-crested waves varies with the phase angle perpendicular to the direction of wave propagation. Later, Zhu and Satravaha [17] extended the study and provided an analytical solution for the velocity potential up to the second-order of wave amplitude.

In this paper, analytical solutions are derived to study the short-crested wave interaction with a concentric porous cylindrical structure in a quantitative manner. It is demonstrated that the analytical method adopted here can investigate the effects of parameters promptly and effectively. Detailed results are presented and discussed on wave forces and surface elevations over a broad range of incident short-crested wave parameters as well as structure configurations including the porosity of the exterior cylinder and the annular gap between the two cylinders. Special attention is paid to the influences of both wave parameters and system configuration on the

wave patterns in the interior domain.

2 Theoretical Formulation

2.1 Governing equations and boundary conditions

In this section, we present the mathematical derivation for a general case of 3D short-crested wave interaction with a concentric porous cylinder system. The solutions for the 2D limiting cases, i.e., a plane incident wave and a standing wave, can be instantly recovered by letting $k_y = 0$ and $k_x = 0$ respectively.

Consider a monochromatic short-crested wave train propagating in the direction of the positive x axis. A structure consisting of two concentric fixed circular cylinders extend from the sea bottom to above the free surface of the ocean along z axis. The origin is placed at the centre of the cylinders on the mean water surface (see Fig. 2). The exterior cylinder is made porous and the interior cylinder is impermeable. The whole fluid region is divided into two regions, the annular region Ω_1 and the region of the outside of the exterior cylinder Ω_2. The following notation have been used in the paper: Φ_j = total velocity potential, Φ^I = velocity potential of incident wave, Φ^S = velocity potential of scattered wave, k = total wave number, k_x = wave number in x direction, k_y = wave number in y direction, ω = wave frequency, h = water depth, A = amplitude of incident wave, a = interior cylinder radius, b = exterior cylinder radius, t = time, ρ = mass density of water, and g = gravitational acceleration. The subscripts $j(j = 1, 2)$ denote the physical parameters in the region $\Omega_j(j = 1, 2)$.

[Fig. 2 about here.]

By assuming that the fluid is inviscid and incompressible, and the flow is irrotational, the fluid motion can be described by a velocity potential Φ_j, which satisfies the Laplace equation

$$\nabla^2 \Phi_j = 0 \qquad \text{in} \quad \Omega_j, \tag{1}$$

subject to the combined linearised free surface boundary condition

$$\Phi_{j,tt} + g\Phi_{j,z} = 0 \qquad \text{at} \quad z = 0, \tag{2}$$

and the bottom condition

$$\Phi_{j,z} = 0 \qquad \text{at} \quad z = -h, \tag{3}$$

where the comma in the subscript designates partial derivative with respect to the variable following it.

The total velocity potential in region Ω_2 can be expressed by the summation of the incident and scattered wave velocity potentials

$$\Phi_2 = \Phi_2^I + \Phi_2^S \qquad \text{in} \quad \Omega_2, \tag{4}$$

where Φ_2^I and Φ_2^S also satisfy (1)-(3).

The velocity potential of the linear short-crested incident wave travelling principally in the positive x direction is given by the real part of [18]

$$\Phi_2^I = -\frac{igA}{\omega} f(z,h) e^{i(k_x x - \omega t)} \cos(k_y y) \qquad \text{in} \quad \Omega_2, \tag{5}$$

where

$$f(z,h) = \frac{\cosh k(z+h)}{\cosh kh}. \tag{6}$$

The term $f(z,h)$ leads to the sea bottom condition being automatically satisfied, while the linearised free surface boundary condition is satisfied using the following dispersion relationship

$$\omega^2 = gk \tanh kh. \tag{7}$$

Assuming that the exterior cylinder is made of fine pores, then the porous flow velocity is linearly proportional to the pressure difference between the two sides of the porous boundary, thus the boundary condition on exterior porous cylinder can be expressed as [5]

$$\Phi_{1,r} = \Phi_{2,r} = iG_0 k(\Phi_1 - \Phi_2) \quad \text{on} \quad r = b, \tag{8}$$

where $G_0 = \frac{\rho\omega d}{\mu}$, is a measure of the porous effect, μ is the coefficient of dynamic viscosity, d is a material constant having the dimension of length. Two special cases corresponding to the two limiting values of the porous effect parameter are: $G_0 = 0$ represents that the boundary is a solid wall, and $G_0 = +\infty$ indicates that the boundary is totally transparent. For typical offshore porous structures, G_0 is normally less than 2.0. More detailed analysis on determination of G_0 value for permeable structures can be found in [19].

The function Φ_2^S in Ω_2 is governed by the Laplace equation (1) with the boundary conditions (2) and (3), the boundary condition at the interface of fluid and porous cylinder at $r = b$, and the radiation condition at infinity, namely, the Sommerfeld condition as follows:

$$\Phi_{2,r}^S = iG_0k(\Phi_1 - \Phi_2^S - \Phi_2^I) - \Phi_{2,r}^I \quad \text{on} \quad r = b, \tag{9}$$

$$\lim_{kr\to\infty} (kr)^{1/2} \left(\Phi_{2,r}^S - ik\Phi_2^S\right) = 0 \qquad \text{in} \quad \Omega_2, \tag{10}$$

where r is the radial axis, and $i = \sqrt{-1}$.

The function Φ_1 in Ω_1 is governed by the Laplace equation (1) with the boundary conditions (2) and (3), and the boundary conditions at the interface of fluid and interior solid cylinder at $r = a$ and exterior porous cylinder at $r = b$:

$$\Phi_{1,r} = 0 \quad \text{on} \quad r = a, \tag{11}$$

$$\Phi_{1,r} = iG_0k(\Phi_1 - \Phi_2^S - \Phi_2^I) \quad \text{on} \quad r = b. \tag{12}$$

These constitute two sets of the governing equation and boundary conditions for the diffraction of short-crested waves by concentric vertical porous cylinder system, corresponding to boundary-value problems in a bounded domain and an unbounded domain respectively. After obtaining Φ_2^S, Φ_2 and Φ_1 by solving the above boundary-value problems, all the physical quantities including the fluid particle velocity, free surface elevation and the dynamic pressure can be calculated respectively from

$$\mathbf{v}_j = \nabla \Phi_j, \tag{13}$$

$$\eta_j = \frac{i\omega}{g} \Phi_j|_{z=0,t=0}, \tag{14}$$

$$p_j = -\rho \Phi_{j,t}. \tag{15}$$

2.2 Analytical solution

The incident wave potential (5) can be written in the cylindrical coordinates as

$$\Phi_2^I = -\frac{igA}{\omega} f(z,h) e^{-i\omega t} \left[\sum_{m=0}^{+\infty} \varepsilon_m i^m J_m(k_x r) \cos(m\theta) \right] \left[\sum_{n=0}^{+\infty} \varepsilon_n J_{2n}(k_y r) \cos(2n\theta) \right], \tag{16}$$

where

$$\varepsilon_m = \begin{cases} 1 & \text{for} \quad m = 0 \\ \\ 2 & \text{for} \quad m \neq 0 \end{cases}, \tag{17}$$

and J_m and J_{2n} are the Bessel function of the first kind of the mth and $2n$th order respectively.

Splitting the product of the two trigonometric functions, (16) becomes

$$\Phi_2^I = -\frac{igA}{2\omega} f(z,h) e^{-i\omega t} \sum_{m=0}^{+\infty} \sum_{n=0}^{+\infty} \varepsilon_m \varepsilon_n i^m J_m(k_x r) J_{2n}(k_y r) \cdot \left[\cos(m+2n)\theta + \cos(m-2n)\theta\right]. \tag{18}$$

The Laplace equation (1) in cylindrical polar coordinates is

$$\frac{1}{r}\frac{\partial}{\partial r}\left(r\frac{\partial \Phi}{\partial r}\right) + \frac{1}{r^2}\frac{\partial^2 \Phi}{\partial \theta^2} + \frac{\partial^2 \Phi}{\partial z^2} = 0. \tag{19}$$

The eigensolutions corresponding to the real and the imaginary eigenvalues can be written as [20]

$$\left\{ \begin{array}{c} H_m^{(1)}(kr) \\ \\ H_m^{(2)}(kr) \end{array} \right\} \left\{ \begin{array}{c} \cos(m\theta) \\ \\ \sin(m\theta) \end{array} \right\} f_0(z), \quad m = 0, 1, 2, 3, \ldots \tag{20}$$

$$\left\{ \begin{array}{c} I_m(k_n r) \\ \\ K_m(k_n r) \end{array} \right\} \left\{ \begin{array}{c} \cos(m\theta) \\ \\ \sin(m\theta) \end{array} \right\} f_n(z), \quad n = 1, 2, 3, \ldots \tag{21}$$

where $H_m^{(1)}$ and $H_m^{(2)}$ are the Hankel functions of the first and second kind, and I_m and K_m are the modified Bessel functions of the first and second kind, respectively. k (wave number) and k_n are the real and imaginary eigenvalues of dispersion relationship (7) respectively, and f_0 and f_n are the real and imaginary eigenfunctions of dispersion relationship (7) respectively.

Considering the form of incident wave potential (18) and boundary conditions, the evanescent waves do not exist in the present problem (See [6] and [15]). Only the

eigensolution (20) is needed to construct the solution forms in this paper.

The solution of the scattered velocity potential in region Ω_2 (Φ_2^S) can be constructed by the following expression [15], which satisfies the Laplace equation (1) and boundary conditions (2), (3), and the Sommerfeld radiation condition (10)

$$\begin{aligned}\Phi_2^S =&\frac{igA}{2\omega}f(z,h)e^{-i\omega t}\sum_{m=0}^{+\infty}\sum_{n=0}^{+\infty}\varepsilon_m\varepsilon_n i^m \\ &\left[A_{mn}^{(1)}H_{m+2n}(kr)\cos(m+2n)\theta + A_{mn}^{(2)}H_{|m-2n|}(kr)\cos(m-2n)\theta\right],\end{aligned} \tag{22}$$

where $A_{mn}^{(1)}$ and $A_{mn}^{(2)}$ are unknown complex coefficients, H_{m+2n} and $H_{|m-2n|}$ are the Hankel functions of the first kind.

Noting the definition $H_m^{(1)}(z) = J_m(z) + iY_m(z)$ and $H_m^{(2)}(z) = J_m(z) - iY_m(z)$ ($Y_m(z)$ are the Bessel functions of the second kind) and the forms of velocity potential in (18) and (22), the solution of the velocity potential in the annular region Ω_1 is constructed as

$$\begin{aligned}\Phi_1 =& -\frac{igA}{2\omega}f(z,h)e^{-i\omega t}\sum_{m=0}^{+\infty}\sum_{n=0}^{+\infty}\varepsilon_m\varepsilon_n i^m\left\{\left[B_{mn}^{(1)}J_{m+2n}(kr)+B_{mn}^{(2)}Y_{m+2n}(kr)\right]\cos(m+2n)\theta\right. \\ &\left.+\left[B_{mn}^{(3)}J_{|m-2n|}(kr)+B_{mn}^{(4)}Y_{|m-2n|}(kr)\right]\cos(m-2n)\theta\right\},\end{aligned} \tag{23}$$

where $B_{mn}^{(1)}$, $B_{mn}^{(2)}$, $B_{mn}^{(3)}$ and $B_{mn}^{(4)}$ are unknown complex coefficients, Y_{m+2n} and $Y_{|m-2n|}$ are the Bessel functions of the second kind. Substituting (18), (22) and (23) into the body boundary conditions (9), (11) and (12), we have

$$B_{mn}^{(1)} J'_{m+2n}(ka) + B_{mn}^{(2)} Y'_{m+2n}(ka) = 0, \tag{24}$$

$$B_{mn}^{(3)} J'_{|m-2n|}(ka) + B_{mn}^{(4)} Y'_{|m-2n|}(ka) = 0, \tag{25}$$

$$\begin{aligned} & k\left[B_{mn}^{(1)} J'_{m+2n}(kb) + B_{mn}^{(2)} Y'_{m+2n}(kb)\right] \\ =& k_x J'_m(k_x b) J_{2n}(k_y b) + k_y J_m(k_x b) J'_{2n}(k_y b) - k A_{mn}^{(1)} H'_{m+2n}(kb) \\ =& iG_0 k\left[B_{mn}^{(1)} J_{m+2n}(kb) + B_{mn}^{(2)} Y_{m+2n}(kb) - J_m(k_x b) J_{2n}(k_y b) + A_{mn}^{(1)} H_{m+2n}(kb)\right], \end{aligned} \tag{26}$$

$$\begin{aligned} & k\left[B_{mn}^{(3)} J'_{|m-2n|}(kb) + B_{mn}^{(4)} Y'_{|m-2n|}(kb)\right] \\ =& k_x J'_m(k_x b) J_{2n}(k_y b) + k_y J_m(k_x b) J'_{2n}(k_y b) - k A_{mn}^{(2)} H'_{|m-2n|}(kb) \\ =& iG_0 k\left[B_{mn}^{(3)} J_{|m-2n|}(kb) + B_{mn}^{(4)} Y_{|m-2n|}(kb) - J_m(k_x b) J_{2n}(k_y b) + A_{mn}^{(2)} H_{|m-2n|}(kb)\right]. \end{aligned} \tag{27}$$

All the unknown coefficients $B_{mn}^{(1)}$, $B_{mn}^{(2)}$, $B_{mn}^{(3)}$, $B_{mn}^{(4)}$, $A_{mn}^{(1)}$, and $A_{mn}^{(2)}$ are obtained explicitly by solving (24)-(27) as

$$B_{mn}^{(1)} = (C_{mn}^{(1)} + C_{mn}^{(2)})/C_{mn}^{(3)}, \tag{28}$$

$$B_{mn}^{(2)} = B_{mn}^{(1)} \cdot \alpha_{mn}, \tag{29}$$

$$B_{mn}^{(3)} = (D_{mn}^{(1)} + D_{mn}^{(2)})/D_{mn}^{(3)}, \tag{30}$$

$$B_{mn}^{(4)} = B_{mn}^{(3)} \cdot \beta_{mn}, \tag{31}$$

$$A_{mn}^{(1)} = C_{mn}^{(4)} \cdot B_{mn}^{(1)} + C_{mn}^{(1)}, \tag{32}$$

$$A_{mn}^{(2)} = D_{mn}^{(4)} \cdot B_{mn}^{(3)} + D_{mn}^{(1)}, \tag{33}$$

where

$$\alpha_{mn} = -\frac{J'_{m+2n}(ka)}{Y'_{m+2n}(ka)}, \tag{34}$$

$$\beta_{mn} = -\frac{J'_{|m-2n|}(ka)}{Y'_{|m-2n|}(ka)}, \tag{35}$$

and

$$C^{(1)}_{mn} = \frac{k_x J'_m(k_x b) J_{2n}(k_y b) + k_y J_m(k_x b) J'_{2n}(k_y b)}{k H'_{m+2n}(kb)}, \tag{36}$$

$$C^{(2)}_{mn} = -\frac{J_m(k_x b) J_{2n}(k_y b)}{H_{m+2n}(kb)}, \tag{37}$$

$$C^{(3)}_{mn} = \left[\frac{1}{H'_{m+2n}(kb)} + \frac{1}{iG_0 H_{m+2n}(kb)}\right]\left[J'_{m+2n}(kb) + \alpha_{mn} Y'_{m+2n}(kb)\right] - \frac{J_{m+2n}(kb) + \alpha_{mn} Y_{m+2n}(kb)}{H_{m+2n}(kb)}, \tag{38}$$

$$C^{(4)}_{mn} = -\frac{J'_{m+2n}(kb) + \alpha_{mn} Y'_{m+2n}(kb)}{H'_{m+2n}(kb)}, \tag{39}$$

$$D^{(1)}_{mn} = \frac{k_x J'_m(k_x b) J_{2n}(k_y b) + k_y J_m(k_x b) J'_{2n}(k_y b)}{k H'_{|m-2n|}(kb)}, \tag{40}$$

$$D^{(2)}_{mn} = -\frac{J_m(k_x b) J_{2n}(k_y b)}{H_{|m-2n|}(kb)}, \tag{41}$$

$$D^{(3)}_{mn} = \left[\frac{1}{H'_{|m-2n|}(kb)} + \frac{1}{iG_0 H_{|m-2n|}(kb)}\right]\left[J'_{|m-2n|}(kb) + \beta_{mn} Y'_{|m-2n|}(kb)\right] - \frac{J_{|m-2n|}(kb) + \beta_{mn} Y_{|m-2n|}(kb)}{H_{|m-2n|}(kb)}, \tag{42}$$

$$D^{(4)}_{mn} = -\frac{J'_{|m-2n|}(kb) + \beta_{mn} Y'_{|m-2n|}(kb)}{H'_{|m-2n|}(kb)}. \tag{43}$$

2.3 Special cases

In this section, the present analytic derivation and solution technique described above are validated via comparisons with existing results reported by other researchers on wave-structure interaction for various combinations of incident (plane and short-crested) waves and structure configurations.

2.3.1 Short-crested wave interaction with a hollow porous cylinder

For the limiting case of short-crested wave interaction with a hollow porous cylinder (i.e., $a = 0$), $\alpha_{mn} = \beta_{mn} = 0$, thus all terms containing α_{mn} and β_{mn} vanish from the solution, i.e.

$$B_{mn}^{(2)} = B_{mn}^{(4)} = 0. \tag{44}$$

2.3.2 Short-crested wave interaction with a solid cylinder

For the limiting case of short-crested wave interaction with a solid cylinder (i.e., $a = 0$, and $G_0 = 0$), $\alpha_{mn} = \beta_{mn} = 0$ and $C_{mn}^{(3)}$=$D_{mn}^{(3)} \to \infty$, thus

$$B_{mn}^{(1)} = B_{mn}^{(2)} = B_{mn}^{(3)} = B_{mn}^{(4)} = 0, \tag{45}$$

$$A_{mn}^{(1)} = C_{mn}^{(1)}, A_{mn}^{(2)} = D_{mn}^{(1)}. \tag{46}$$

Therefore $\Phi_1 = 0$ indicating there is no wave in the inner region Ω_1 and the solution of Φ_2^S is exactly the same as equation (19) given in [15].

2.3.3 *Plane wave interaction with a concentric porous cylindrical structure*

For the limiting case of a plane wave interaction with a concentric porous cylindrical structure (i.e., $k_y = 0$ and $k = k_x$), $J_0(k_y b) = 1$, $J_{2n}(k_y b) = 0$ ($n = 1, 2, 3 \cdots$), and $J'_{2n}(k_y b) = 0$ ($n = 0, 1, 2 \cdots$), thus coefficients $A^{(1)}_{mn}$, $A^{(2)}_{mn}$, $B^{(1)}_{mn}$, $B^{(2)}_{mn}$, $B^{(3)}_{mn}$, $B^{(4)}_{mn}$ ($n \neq 0$) vanish and the series in (22) and (23) change from double series to single series. The remaining coefficients can be simplified as

$$\alpha_{m0} = \beta_{m0} = -\frac{J'_m(ka)}{Y'_m(ka)}, \tag{47}$$

$$C^{(1)}_{m0} = D^{(1)}_{m0} = \frac{J'_m(kb)}{H'_m(kb)}, \tag{48}$$

$$C^{(2)}_{m0} = D^{(2)}_{m0} = -\frac{J_m(kb)}{H_m(kb)}, \tag{49}$$

$$C^{(3)}_{m0} = D^{(3)}_{m0} = -\frac{H'_m(kb)S_m + \frac{2iG_0}{\pi kb H'_m(ka)}}{iG_0 H_m(kb) H'_m(kb) Y'_m(ka)}, \tag{50}$$

$$C^{(4)}_{m0} = D^{(4)}_{m0} = \frac{S_m}{H'_m(kb)Y'_m(ka)}, \tag{51}$$

where $S_m = J'_m(ka)Y'_m(kb) - J'_m(kb)Y'_m(ka)$.

Then the coefficients $B^{(1)}_{mn}$, $B^{(2)}_{mn}$, $B^{(3)}_{mn}$, $B^{(4)}_{mn}$, $A^{(1)}_{mn}$, and $A^{(2)}_{mn}$ are solved as

$$B^{(1)}_{m0} = B^{(3)}_{m0} = -\frac{\frac{2G_0}{\pi kb}Y'_m(ka)}{T_m}, \tag{52}$$

$$B^{(2)}_{m0} = B^{(4)}_{m0} = \frac{\frac{2G_0}{\pi kb}J'_m(ka)}{T_m}, \tag{53}$$

$$A^{(1)}_{m0} = A^{(2)}_{m0} = \frac{J'_m(kb)S_m + \frac{2iG_0}{\pi kb}J'_m(ka)}{T_m}, \tag{54}$$

where $T_m = H'_m(kb)S_m + \frac{2iG_0}{\pi kb}H'_m(ka)$.

The solutions of Φ_1 and Φ_2^S are now exactly the same as equations (16) and (13)

in [10]. It is noted that the Wronskian identity $J_m(z)Y'_m(z)-Y_m(z)J'_m(z) = 2/(\pi z)$ and equation $H_m(z) = J_m(z) + iY_m(z)$ are used in the above simplification.

2.3.4 Plane wave interaction with a hollow porous cylinder

The solution for the limiting case of plane wave interaction with a hollow porous cylinder (i.e., $k_y = 0$, $k = k_x$ and $a = 0$), is obtained by simply taking the limit of (52)-(54) as $a \to 0$, the coefficients become

$$B_{m0}^{(1)} = B_{m0}^{(3)} = \frac{\frac{2G_0}{\pi kb}}{H'_m(kb)J'_m(kb) + \frac{2G_0}{\pi kb}}, \tag{55}$$

$$B_{m0}^{(2)} = B_{m0}^{(4)} = 0, \tag{56}$$

$$A_{m0}^{(1)} = A_{m0}^{(2)} = \frac{[J'_m(kb)]^2}{H'_m(kb)J'_m(kb) + \frac{2G_0}{\pi kb}}. \tag{57}$$

These coefficients are exactly the same as in equations (24)-(26) reported in [10] considering the different sign of Φ_2^S.

2.4 Physical properties

All the other physical properties of engineering interest including velocity, surface elevation, and pressure can now be determined based on the velocity potentials by (13)-(15). The total force, per unit height in the direction of wave propagation is

$$\frac{dF_x}{dz} = -R\int_0^{2\pi} p \cdot \cos(\theta) d\theta = P(k_x, k_y, k, R) \cdot \rho g A R \cdot f(z,h) e^{-i\omega t}, \tag{58}$$

where

$$P(k_x, k_y, k, R) = -2\pi i \left[P_0(k_x, k_y, k, R) + \sum_{n=0}^{+\infty} P_n(k_x, k_y, k, R) \right], \tag{59}$$

$$P_0(k_x, k_y, k, a) = B_{1,0}^{(1)} J_1(ka) + B_{1,0}^{(2)} Y_1(ka), \tag{60}$$

$$P_n(k_x, k_y, k, a) = (-1)^n [(B_{2n+1,n}^{(3)} - B_{2n-1,n}^{(3)}) J_1(ka) + (B_{2n+1,n}^{(4)} - B_{2n-1,n}^{(4)}) Y_1(ka)], \tag{61}$$

$$P_0(k_x, k_y, k, b) = J_1(k_x b) J_0(k_y b) - A_{1,0}^{(1)} H_1(kb) - B_{1,0}^{(1)} J_1(kb) - B_{1,0}^{(2)} Y_1(kb), \tag{62}$$

$$\begin{aligned} P_n(k_x, k_y, k, b) =& (-1)^n \Big\{ [J_{2n+1}(k_x b) - J_{2n-1}(k_x b)] J_{2n}(k_y b) - (A_{2n+1,n}^{(2)} - A_{2n-1,n}^{(2)}) H_1(kb) \\ & - [(B_{2n+1,n}^{(3)} - B_{2n-1,n}^{(3)}) J_1(kb) + (B_{2n+1,n}^{(4)} - B_{2n-1,n}^{(4)}) Y_1(kb)] \Big\}, \end{aligned} \tag{63}$$

where the function $P(k_x, k_y, k, R)$ is a dimensionless parameter of $\frac{dF_x}{dz}$ without the term $\rho g A R \cdot f(z, h) e^{-i\omega t}$ and R denotes the radii of the cylinders (a or b).

The inertia coefficient C_M and linear drag coefficient C_D per unit height are defined as [20]

$$\mathrm{Re}\left(\frac{dF_x}{dz} \right) = \rho \pi R^2 \left(C_M \dot{U} + \omega C_D U \right), \tag{64}$$

where U is the velocity of the incident waves at the origin of the cylinder in its absence.

From (5), (58) and (64), we have

$$C_M = -\frac{P_i}{\pi k_x R}, \quad C_D = \frac{P_r}{\pi k_x R}, \tag{65}$$

where P_r and P_i are the real and imaginary parts of $P(k_x, k_y, k, R)$ respectively.

It can be concluded from (65) that, the total force without the term $\rho g A R \cdot f(z,h)e^{-i\omega t}$ is

$$|P| = \pi k_x R \sqrt{C_M^2 + C_D^2}. \tag{66}$$

3 Results and discussion

3.1 Influence of the porosity of the exterior cylinder

The wave force exerted on the interior and exterior cylinders for the exterior cylinder of different porosity (G_0) is calculated and results are presented in Figs. 3 and 4 respectively, where $ka = 1$ and $b/a = 4$. Four cases of incident waves with increasing short-crestedness are presented in the figures: (1) $k_x a = 1$, $k_y a = 0$; (2) $k_x a = 0.8$, $k_y a = 0.6$; (3) $k_x a = k_y a = \sqrt{2}/2$; and (4) $k_x a = 0.6$, $k_y a = 0.8$. It can be seen that, as porous parameter G_0 increases, the total nondimensional horizontal force on the interior cylinder increases monotonically while the total force on the exterior cylinder decreases monotonically. The variation in forces is slow at higher G_0, and appeared to approach their asymptotic values in each case respectively.

[Fig. 3 about here.]

[Fig. 4 about here.]

The influence of the porous-effect parameter G_0 on linear wave runups is shown in Figs. 5 - 7 with radii ratio of $b/a = 4$ and $k_x a = k_y a = \sqrt{2}/2$. Three cases of the exterior cylinder with different porous parameter $G_0 =$ 1/2, 1 and 2 are presented in the figures. In the annular region Ω_1, it is clearly seen that the linear wave runups increase on both the interior cylinder and exterior cylinder as G_0 increases except in the lee side region of the exterior cylinder (about $[-\pi/6, \pi/6]$) where η/A to be insensitive to G_0, showing that the higher porosity of the exterior cylinder clearly results in higher wave transmission into the inner region (Figs. 5 and 6). On the outer unbounded region Ω_2, however, no uniform clear trend on the linear wave runup on the exterior cylinder is observed. Instead the linear wave runup tends to increase with the increasing porosity in the lee side of the exterior cylinder while it appears to decrease as G_0 increases near the front of the cylinder (Fig. 7).

[Fig. 5 about here.]

[Fig. 6 about here.]

[Fig. 7 about here.]

3.2 Influence of annular spacing

The effect of the annular spacing between the cylinders is investigated and the results are presented in terms of the nondimensional total force variation on the ratio a/b in Figs. 8 and 9 for a given $k_x b$. The wave number ratio representing the short-crestedness k_y/k_x is ranged from 0 to 1 with an interval of 0.2. For a fixed nondimensional radius of the exterior cylinder $k_x b$, Fig. 8 shows lower wave

force on the interior cylinder with smaller $k_x a$ when the annular spacing is large (or small a/b). Also, the nondimensional total horizontal force on the interior cylinder increases monotonously for small $k_x a$ and a fluctuation pattern is observed for large $k_x a$. A clear trend of decreasing wave force on the interior cylinder as the incident wave become more short-crested is observed in the figure.

[Fig. 8 about here.]

Fig. 9(a) shows that the wave forces on the exterior cylinder $|P_b|$ resulted from short-crested waves ($k_x b = 1$) are normally lower than that from the plane incident wave for large annular spacing (or small a/b). Maximum wave forces appear to occur at the largest annular spacing ($a/b = 0$) for all wave conditions, corresponding to the case of a single hollow cylinder. It is seen that a trough of zero value emerges for higher k_y/k_x while the result from a plane incident wave only has one trough occurring at $a/b = 1$, corresponding to the minimum spacing. However, the variations, shown in Fig. 9(b) of the nondimensional total horizontal forces on the exterior cylinder $|P_b|$ for $k_x b = 2$ are quite different for different k_y/k_x values and the maximum wave forces are seen to occur near the ratio of $a/b = 0.5$. In contrast to the case of $k_x b = 1$, wave forces resulting from the hollow porous cylinder do not reach its maximum, and tend to increase with increasing short-crestedness of the incident waves. Therefore, wave forces resulting from a concentric cylinder system are not only dependent on the configuration but also on the incident wave conditions. Further study into the identification of the occurrence of the minimum and maximum wave forces could lead to significant improvement for engineering design to minimise the hydrodynamic loads on real marine structures.

[Fig. 9 about here.]

3.3 Influence of wave parameters

The variation of the nondimensional total horizontal forces $|P|$ on the interior and exterior cylinders vs. k_y/k_x for different $k_x a$ values ($k_x a$ varies from 0.05 to 1.0) , $b/a = 4$ is shown in Figs. 10 and 11. The results are calculated for the porous effect parameter of the exterior cylinder $G_0 = 1$. As can be seen in Fig. 10, wave forces on the interior cylinder decreases sharply with the increasing short-crestedness (k_y/k_x) for the two large $k_x a$ values accompanied with significant fluctuation. However, at low $k_x a$, wave forces remain relative small and less dependent on the short-crestedness of the incident waves. Fig. 11 shows the variation of the nondimensional wave force on the exterior porous cylinder on the short-crestedness of the incident waves. It is clear seen that, in addition to the general trend of decreasing wave force with increasing short-crestedness, there are troughs for all $k_x a$ values plotted indicating extremely low wave forces on the exterior cylinder. It is interesting to note that, for a given $k_x a$, while the wave force on the interior cylinder reaches a peak, the exact same short-crestedness of the incident wave leads to the minimum wave force on the exterior cylinder (trough), and vice versa. However, the short-crestedness corresponding to the minimum wave force on the interior cylinder does not appear to be the same at which the force on the exterior cylinder reaches a peak. This variation of maximum wave forces on the interior and exterior cylinders provides an effective means of minimising wave loads on both cylinders. This important characteristic in the forces can be effectively applied in a design to reduce the wave impact on coastal and offshore porous structures.

[Fig. 10 about here.]

[Fig. 11 about here.]

3.4 Surface elevation

It is interesting to study the changes in the wave surface elevation in the annular region of the concentric porous cylindrical structure for varying incident wave parameters and structure configuration. Fig. 12 shows the resulting wave amplitude and corresponding phase contours resulting from plane, short-crested, and standing incident waves interaction with the structure for configuration parameters: $G_0 = 1.0$, $k = 1\,\mathrm{m}^{-1}$, $a = 1\,\mathrm{m}$ and $b/a = 4$. The amplitudes shown in Figs. 12 and 13 are nondimensionalised as $|\eta|/A$, and the phase values plotted are in the range of $[-\pi \sim +\pi]$.

It is clear that the diffracted wave patterns of short-crested waves are more complex than those of plane waves. As one will expect, all the equi-amplitude plots are symmetric with respect to the longitudinal (x) axis leading to zero force in transverse (y) direction. Moreover, the diffracted wave pattern resulting from a standing wave shown in Fig. 12 is symmetric in both x and y planes, generating zero horizontal force in both longitudinal and transverse directions. From Fig. 12, it is seen that the amplitude of the diffracted short-waves in the weather region is smaller than that of a plane wave, and the region for the large amplitude waves in front of the interior cylinder resulting from short-crested waves is also smaller than its plane wave counterpart. Such tendencies are more pronounced as the incident waves become more short-crested.

The thick lines in phase contours represent changes from π to $-\pi$. The amphidromic points, where equi-phase lines converge and the wave amplitude vanishes, are seen clearly formed for short-crested incident waves. Similar to the feature observed by Zhu [15] for short-crested wave diffraction by a single impermeable cylinder, the

phases near two adjacent amphidromic points rotate from $-\pi$ to $+\pi$ clockwise and counter-clockwise around the amphidromic points respectively in the annular region. The density of the amphidromic points increases as the wave crests become shorter. As one would expect for the standing incident wave component, the amplitude and phase contours maintain symmetry in the x- and y-plane. The amplitudes in the transverse directions are small compared to their inline values, with a faster variation in the corresponding phase contours.

[Fig. 12 about here.]

Fig. 13 shows the short-crested wave amplitude and phase contours resulting from different annular spacing for $G_0 = 1.0$, $k_x = k_y = \sqrt{2}/2$ m^{-1}, and $a = 1$ m. As can be seen in Fig. 13, there is no clear trend on the wave pattern on the annular spacing. The symmetry to the x axis of both amplitude and phase contour patterns are preserved. As the annular spacing increases, the wave patterns in the annular region becomes more complex, with increases in density of the both amplitude and phase contours. This is main due to more physical space for the waves transmitted into the annular region to develop. On the other hand, however, in the smallest annular region shown in Fig. 13 ($b/a = 2$), the amphidromic points can no longer form due to the small confined area.

[Fig. 13 about here.]

It is worth to note that the analytical derivation and results presented in this paper are limited to linear short-crested waves. Since short-crested waves commonly arise from the oblique interaction of two travelling plane waves, hence linear solutions for short-crested waves are also achievable by linear superposition from the plane wave case. However, as a first step of completely solving the short-crested wave interaction with the complex concentric porous cylinder system, the methodology

and theoretical approach presented in the paper is a crucial step and will lead to the further extension to solve the nonlinear short-crested wave diffraction problem.

4 Conclusions

A general 3D short-crested wave interaction with a concentric porous cylinder system is solved. Based on potential theory, fully analytical solution is obtained. It is found that the porous-effect parameter should be chosen less than 2 in order to provide meaningful protection to the interior cylinder from wave impact as the wave force on the interior cylinder increases sharply from $G_0 = 0$ to 2. On the other hand, the wave forces on the interior cylinder can be significantly reduced by reducing the annular spacing between the two cylinders. Identification of the peaks and troughs of the wave forces are presented in order to minimise the wave impact on the cylinders, especially on the interior cylinder. These findings can directly lead to significant improvement in practical design of marine structures. Results on surface elevations in the annular region should also be found useful in the design of coastal and offshore structures.

5 Acknowledgment

This paper is based on the project funded by Australian Research Council (ARC) under Discovery Project Grant No. DP0450906. Authors would like to thank the financial support from ARC.

References

[1] Vijayalakshmi K, Neelamani S, Sundaravadivelu R, Murali K. Wave runup on a concentric twin perforated circular cylinder. Ocean Engineering 2007;34(2):327-36.

[2] Taylor G. Fluid flow in regions bounded by porous surfaces. Proceedings of the Royal Society of London, Series A 1956;234:456-75.

[3] Molin B, Legras JL. Hydrodynamic modeling of the Rouseau tower stabilizer. In: 9th International Conference on Offshore Mechanics and Arctic Engineering. 1990.

[4] Le Bris F, Marichal D. Numerical and experimental study of submerged supple nets: Applications to fish farms. Journal of Marine Science and Technology 1998;3:161-70.

[5] Chwang AT. A porous wavemaker theory. Journal of Fluid Mechanics 1983;132:395-406.

[6] Yu X, Chwang AT. Wave-induced oscillation in harbor with porous breakwaters. Journal of Waterway, Port, Coastal, and Ocean Engineering 1994;120(2):125-44.

[7] Yu X, Chwang AT. Wave motion through porous structures. Journal of Engineering Mechanics 1994;120(5):989-1008.

[8] Chwang AT, Chan AT. Interaction between porous media and wave motion. Annual Review of Fluid Mechanics 1998;30:53-84.

[9] Wang KH, Ren X. Water waves on flexible and porous breakwater. Journal of Engineering Mechanics 1993;119(5):1025-47.

[10] Wang KH, Ren X. Wave interaction with a concentric porous cylinder system. Ocean Engineering 1994;21(4):343-60.

[11] Li Y, Sun L, Teng B. Wave action on double-cylinder structure with perforated outer wall. In: 22nd International Conference on Offshore Mechanics and Arctic Engineering. 2003. CD-ROM: OMAE2003-37094.

[12] Darwiche MKM, Williams AN, Wang KH. Wave interaction with semiporous cylindrical breakwater. Journal of Waterway, Port, Coastal, and Ocean Engineering 1994;120(4):382-403.

[13] Williams AN, Li W. Wave interaction with a semi-porous cylindrical breakwater mounted on a storage tank. Ocean Engineering 1998;25(2-3):195-219.

[14] Tsai CP, Jeng DS, Hsu JRC. Computations of the almost highest short-crested waves in deep water. Applied Ocean Research 1994;16(6):317-26.

[15] Zhu S. Diffraction of short-crested waves around a circular cylinder. Ocean Engineering 1993;20(4):389-407.

[16] Zhu S, Moule G. Numerical calculation of forces induced by short-crested waves on a vertical cylinder of arbitrary cross-section. Ocean Engineering 1994;21(7):645-62.

[17] Zhu S, Satravaha P. Second-order wave diffraction forces on a vertical circular cylinder due to short-crested waves. Ocean Engineering 1995;22(2):135-89.

[18] Fuchs RA. On the theory of short-crested oscillatory waves. In: Gravity Waves, National Bureau of Standards Circular No. 521, Department of Commerce, USA. 1952. p.187-200.

[19] Li Y, Liu Y, Teng B. Porous effect parameter of thin permeable plates. Coastal Engineering Journal 2006;48(4):309-36.

[20] Mei CC. The applied dynamics of ocean surface waves. Singapore: World Scientific;1989.

List of Figures

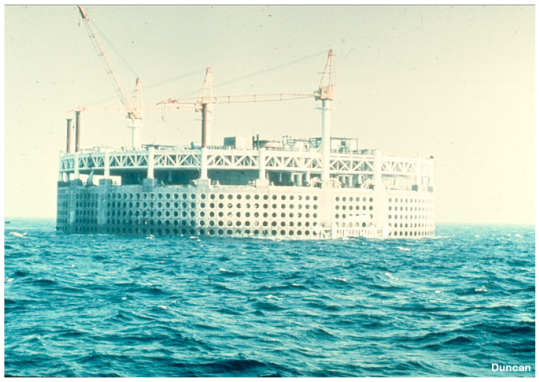

Fig. 1. Ekofisk Gravity Structure (Courtesy ConocoPhillps).

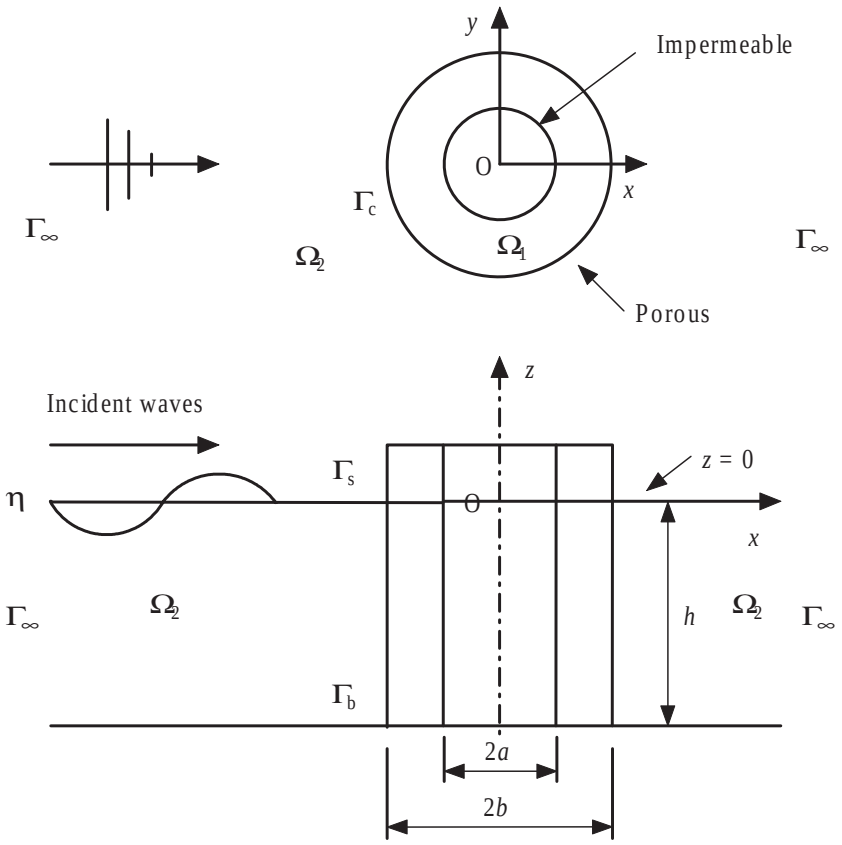

Fig. 2. Definition sketch of wave interaction with a concentric porous cylindrical structure

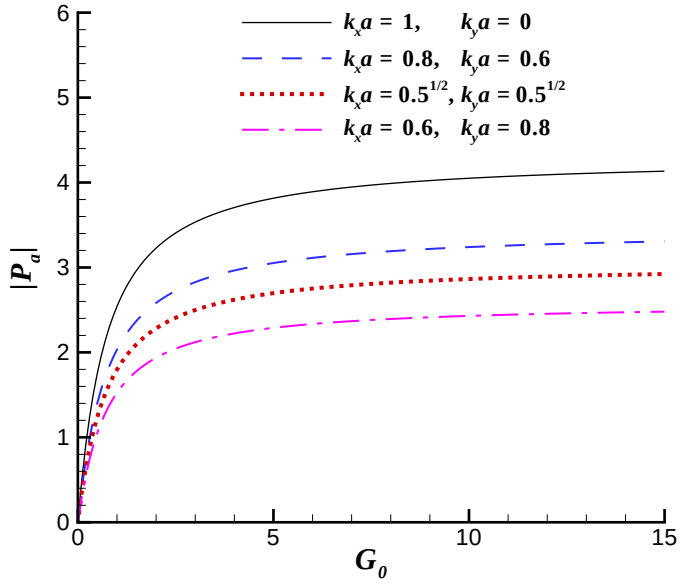

Fig. 3. Variations of the nondimensional total horizontal force of the interior cylinder $vs.$ the porous-effect parameter G_0 ($b/a = 4$ and $ka = 1$).

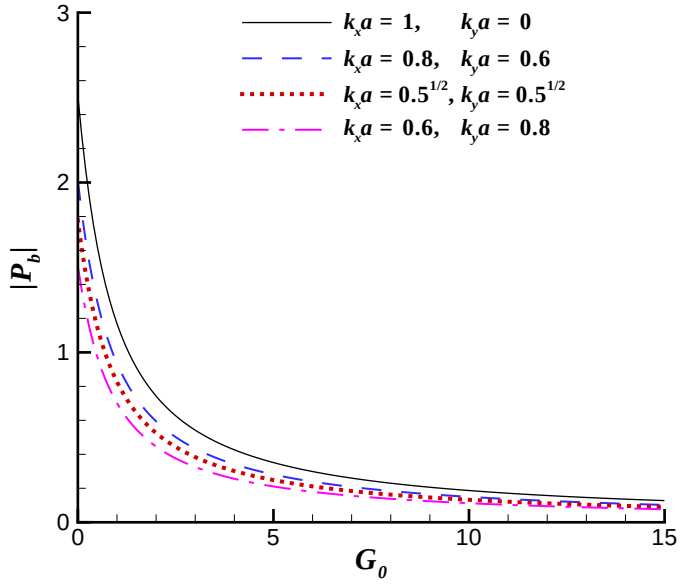

Fig. 4. Variations of the nondimensional total horizontal force of the exterior cylinder $vs.$ the porous-effect parameter G_0 ($b/a = 4$ and $ka = 1$).

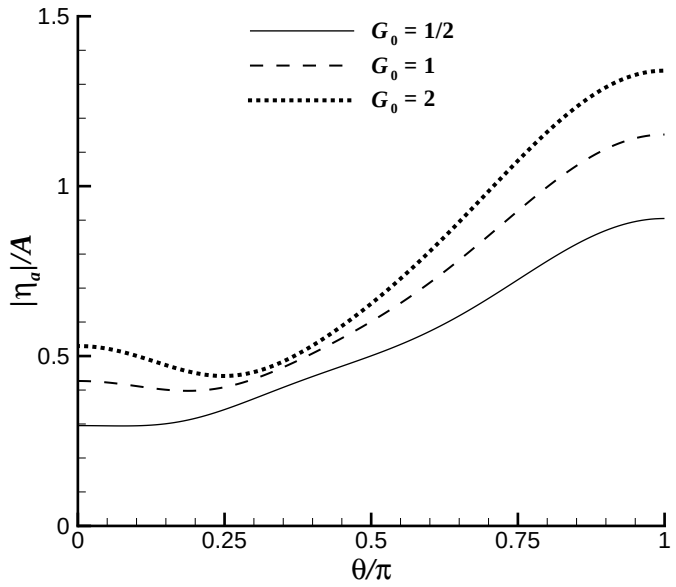

Fig. 5. The nondimensional linear runup around the interior cylinder with different porous–effect parameter G_0 ($b/a = 4$ and $k_x a = k_y a = \sqrt{2}/2$).

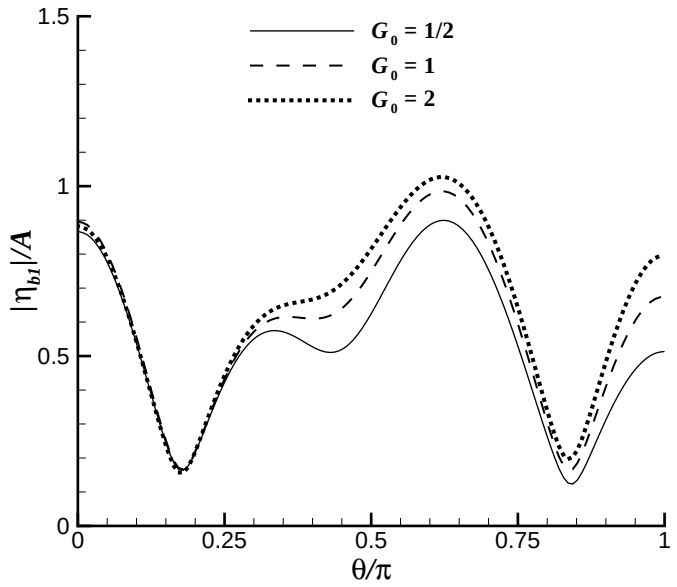

Fig. 6. The nondimensional linear runup around the exterior cylinder (in Ω_1) with different porous-effect parameter G_0 ($b/a = 4$ and $k_x a = k_y a = \sqrt{2}/2$).

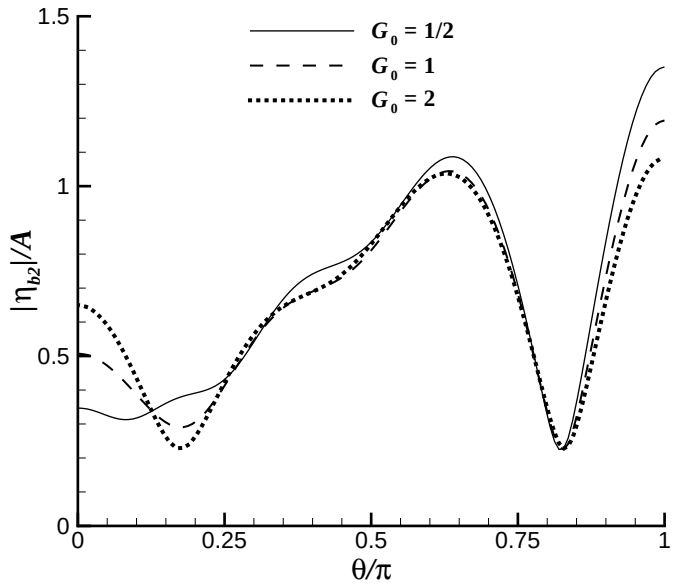

Fig. 7. The nondimensional linear runup around the exterior cylinder (in Ω_2) with different porous-effect parameter G_0 ($b/a = 4$ and $k_x a = k_y a = \sqrt{2}/2$).

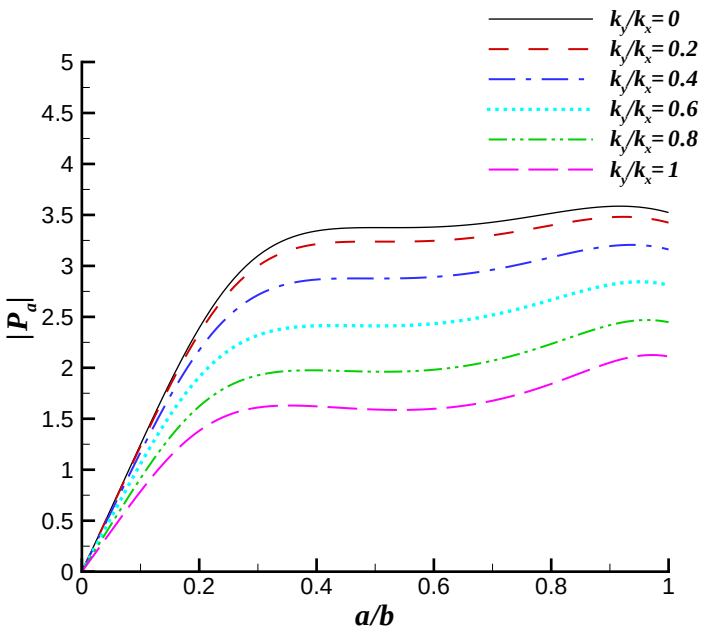

Fig. 8. Variation of the nondimensional total horizontal force on the interior cylinder $vs.$ the ratio a/b at different k_y ($k_x b = 2$).

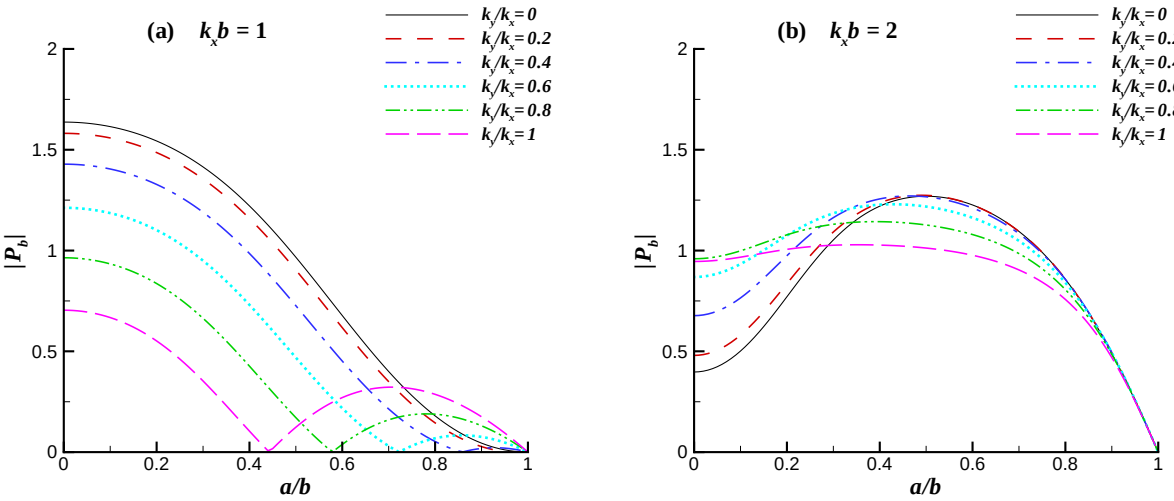

Fig. 9. Variation of the nondimensional total horizontal force on the exterior cylinder $vs.$ the ratio a/b at different k_y ($k_x b = 1$ and 2).

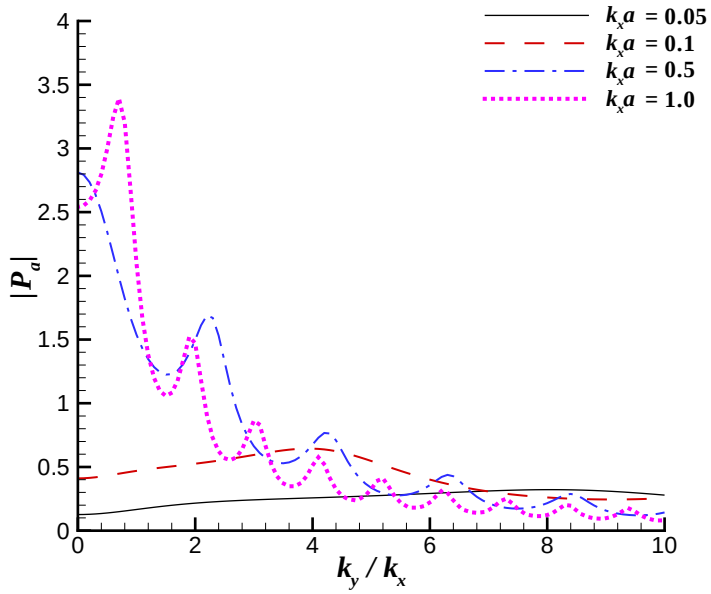

Fig. 10. Variation of the nondimensional total horizontal force on the interior cylinder $vs.$ the ratio k_y/k_x at $b/a = 4$ and $G_0 = 1$.

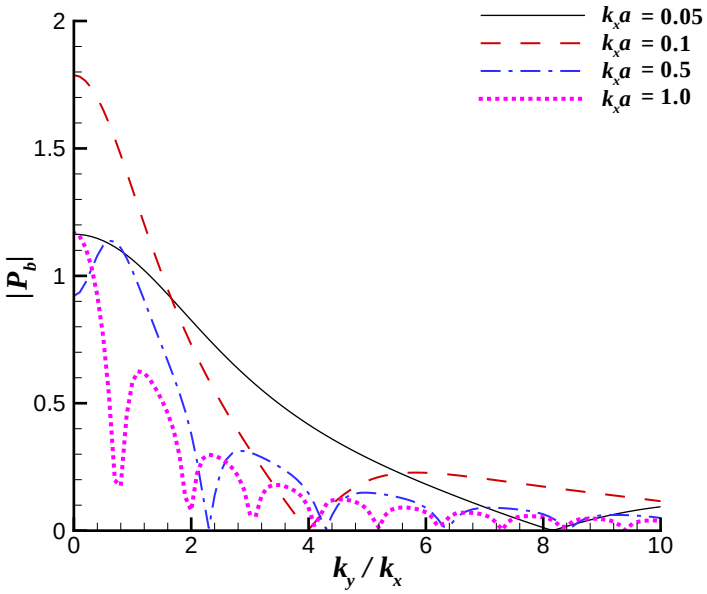

Fig. 11. Variation of the nondimensional total horizontal force on the exterior cylinder $vs.$ the ratio k_y/k_x at $b/a = 4$ and $G_0 = 1$.

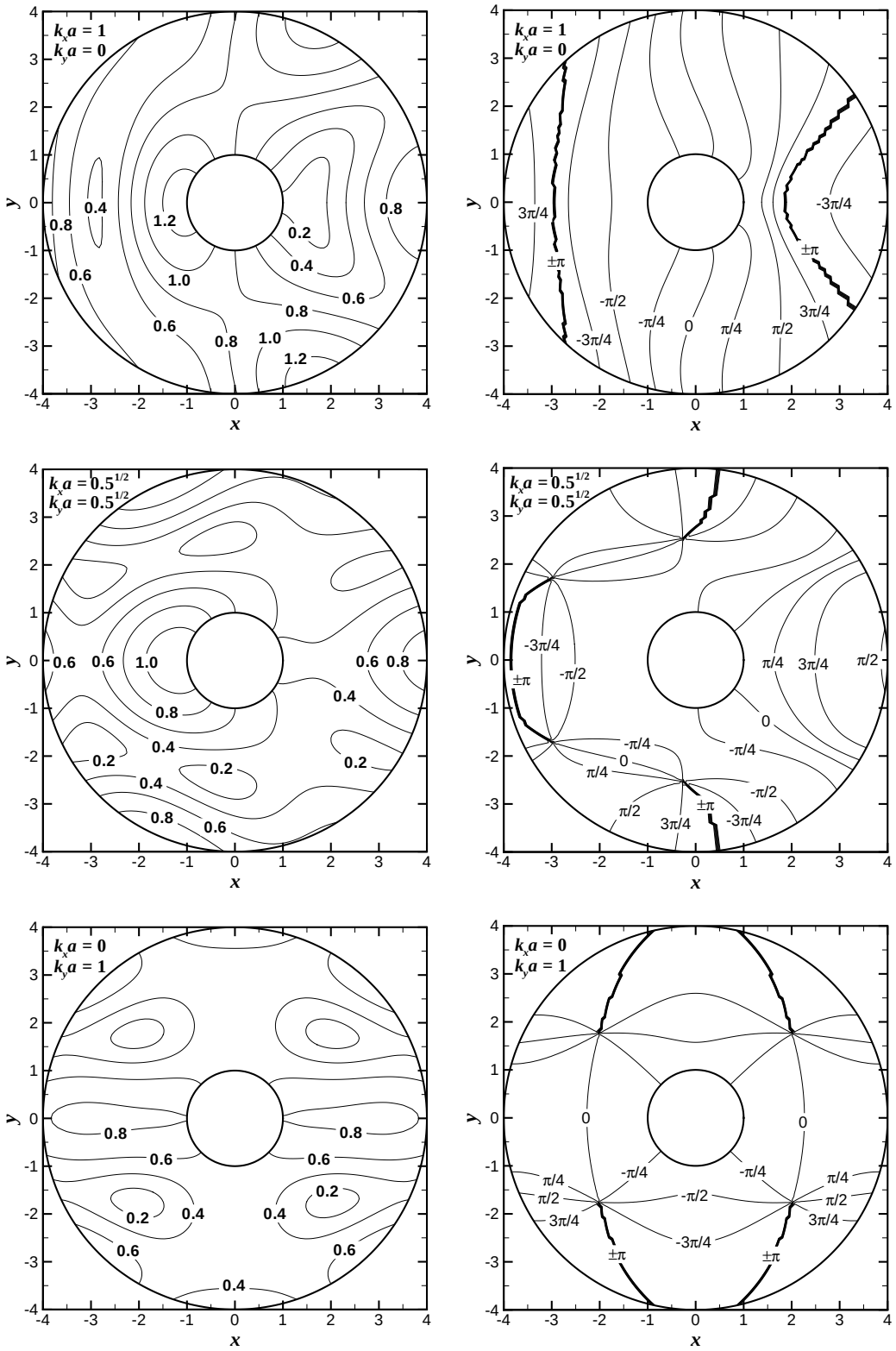

Fig. 12. Equi-amplitude (left) and Equi-phase (right) contours for incident short-crested wave with $b/a = 4$, $G_0 = 1$, $k = 1$ m^{-1} and $a = 1$ m.

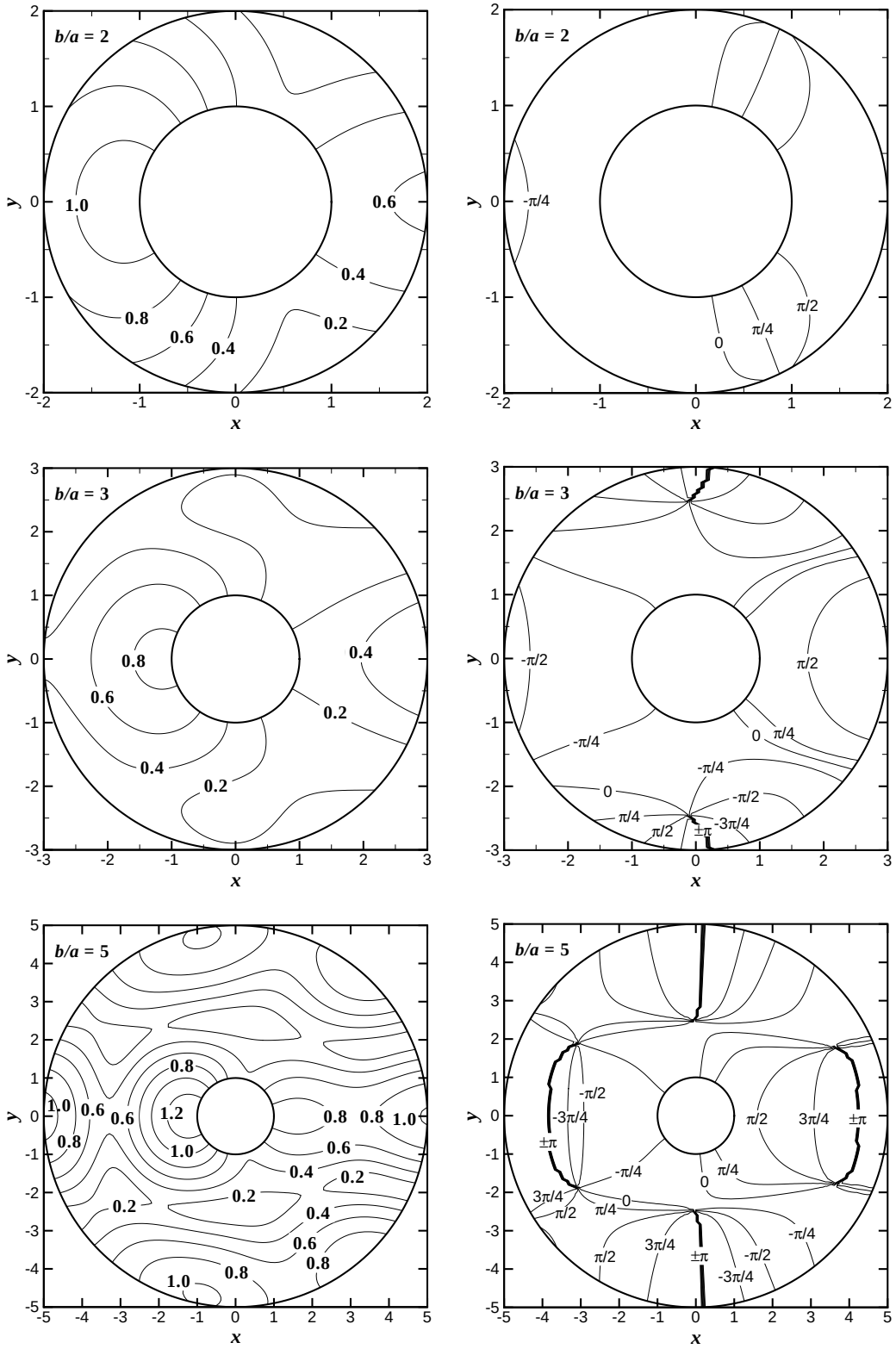

Fig. 13. Equi-amplitude (left) and Equi-phase (right) contours for incident short-crested wave with $k_x = k_y = \sqrt{2}/2$ m^{-1}, $a = 1$ m and $G_0 = 1$.